

1  
2  
3  
4  
5  
6  
7  
8  
9  
10  
11  
12  
13  
14  
15  
16  
17  
18  
19

# **Emergent low-frequency activity in cortico-cerebellar networks with motor skill learning**

Pierson J. Fleischer<sup>1</sup>, Aamir Abbasi<sup>1</sup>, Andrew W. Fealy<sup>1</sup>, Nathan P. Danielsen<sup>1</sup>,  
Ramneet Sandhu<sup>1</sup>, Philip R. Raj<sup>1</sup>, Tanuj Gulati<sup>1,2,3 #</sup>

<sup>1</sup> Center for Neural Science and Medicine, Department of Biomedical Sciences, Cedars-Sinai Medical Center, Los Angeles, CA.

<sup>2</sup> Department of Neurology, Cedars-Sinai Medical Center, Los Angeles, CA.

<sup>3</sup> Department of Medicine, David Geffen School of Medicine; and Department of Bioengineering, Henry Samueli School of Engineering, University of California-Los Angeles, Los Angeles, CA.

# Correspondence: [tanuj.gulati@csmc.edu](mailto:tanuj.gulati@csmc.edu)

20 **Abstract**

21

22 The motor cortex controls skilled arm movement by recruiting a variety of targets in the nervous  
23 system, and it is important to understand the emergent activity in these regions as refinement of  
24 a motor skill occurs. One fundamental projection of the motor cortex is to the cerebellum.  
25 However, the emergent activity in the motor cortex and the cerebellum that appears as a  
26 dexterous motor skill is consolidated is incompletely understood. Here, we report on low-  
27 frequency oscillatory (LFO) activity that emerges in cortico-cerebellar networks with learning the  
28 reach-to-grasp motor skill. We chronically recorded the motor and the cerebellar cortices in rats  
29 which revealed the emergence of coordinated movement-related activity in the local-field  
30 potentials (LFPs) as the reaching skill consolidated. We found that the local and cross-area  
31 spiking activity was coordinated with LFOs. Finally, we also found that these neural dynamics  
32 were more prominently expressed during accurate behavior. This work furthers our understanding  
33 on emergent dynamics in the cortico-cerebellar loop that underlie learning and execution of  
34 precise skilled movement.

35

36

37 **Keywords:** Motor cortex, cerebellum, oscillations, skill learning.

## 38 Introduction

39  
40 The primary motor cortex (M1) is viewed as a driver for movement and an emerging view posits  
41 transient oscillatory dynamics- both at the level of spiking and local field potentials (LFPs) as the  
42 neural substrate for it<sup>1-7</sup>. There has been a particular interest in low-frequency quasi-oscillatory  
43 activity (LFOs) in M1, which can be brief (1-2 cycles) for rapid movements or longer for sustained  
44 movements, and it has been shown to be phase-locked to sub-movement timing<sup>2,3,8,9</sup>. Recent  
45 work showed that such oscillatory dynamics are coordinated in the M1 and dorsolateral striatum  
46 in the rodents as they learned a reach-to-grasp task<sup>3</sup>. One of M1's principal projections is to the  
47 cerebellum via the pons<sup>10-13</sup>, but similar oscillatory dynamics have not been studied in cortico-  
48 cerebellar networks.

49  
50 M1 is a key brain hub involved in voluntary forelimb movement: experimental lesions of M1 in  
51 animal models or neurological injury to M1 (such as stroke) impair dexterity<sup>2,14-16</sup>, stimulation of  
52 M1 neurons evokes movement<sup>17-19</sup>, spiking activity in M1 is closely linked to movement  
53 parameters<sup>3,11,20-23</sup> and optogenetic perturbation of M1 affects forelimb behaviors<sup>18,20,24,25</sup>. The  
54 cerebellum's role in the coordination of arm movements has also been extensively studied.  
55 Investigation of prehension/reaching tasks in animals have shown that cerebellar neurons – both  
56 in the cerebellar cortex and its deep nuclei are tuned to several movement-related events such  
57 as movement onset, cues leading to movement and its duration, limb position, velocity and muscle  
58 activity<sup>26-31</sup>. Besides coding for the above-listed features of limbs and associated movement  
59 parameters, other evidence indicates that the cerebellum participates in the formation of  
60 procedural memories, learning and retention of skills, habits, and conditioned responses<sup>32,33</sup>.  
61 Cerebellar lesions impair acquisition of skilled behaviors and patients with cerebellar disease  
62 show impaired reaching<sup>34-36</sup>. Furthermore, optogenetic perturbation of cerebellar nuclei or pontine  
63 inputs can cause a loss of endpoint precision in mice during reach-to-grasp behavior<sup>13,37</sup>.

64 Additionally, electric stimulation over the cerebellum facilitates adaptive control of reaching<sup>38,39</sup>.  
65 Recent rodent work using two-photon imaging showed the emergence of shared neuronal-  
66 dynamics in *M1*-cerebellar ensembles as animals learned to expertly control a manipulandum<sup>11</sup>.  
67  
68 In this study, we have focused on transient oscillatory dynamics that emerge in M1 and the  
69 cerebellum as a reaching skill is learned. We recorded neural activity in the M1 and contralateral  
70 cerebellum (the primary M1 target through pons nuclei) throughout the learning of a reach-to-  
71 grasp skill in rats. We observed emergent coordinated low-frequency oscillatory activity (1-4 Hz)  
72 across M1 and cerebellum LFPs that was linked to increased success rates. We also found that  
73 LFPs modulated spiking in both regions and that the spiking dynamics were conserved for  
74 successful, accurate movements.

## 75 **Results**

76

77 We trained 13 rats on the Whishaw forelimb reach-to-grasp task<sup>40,41</sup> in our in-house built  
78 automated training box that is compatible with electrophysiology (**Fig. 1A**)<sup>2,41,42</sup>. We chose this  
79 task due to its similarity to skilled learning tasks in humans<sup>43,44</sup> as well as extensive evidence that  
80 this task is associated with multiple levels of neural plasticity in the M1 and the cerebellum.  
81 Examples of this include changes in Long-Term Potentiation (LTP)<sup>45</sup>, dendritic spine growth<sup>46</sup>  
82 motor map plasticity in the M1<sup>47</sup>, as well as patterned spiking in the cerebellar cortex<sup>29</sup> and more  
83 recently, it has also been demonstrated that cerebellar associative learning underlies reach  
84 adaptation<sup>48</sup>. Importantly, patients with neurologic injury in either region show impairment in this  
85 skilled reaching behavior<sup>36,49</sup>. In a subset of rats ( $n = 5$ ) that were monitored during reach-to-grasp  
86 motor skill consolidation, we also recorded neural signals, including single-unit activity and local  
87 field potentials (LFPs) in M1 and cerebellum (**Fig. 2A**). For the electrophysiology experiments,  
88 microelectrodes were implanted (microwire arrays in M1 and tetrodes/ polytrodes in cerebellum,  
89 see Materials and Methods; and **Supplementary Table 1**). In the animals that were recorded,  
90 training began five days after electrode placement surgery.

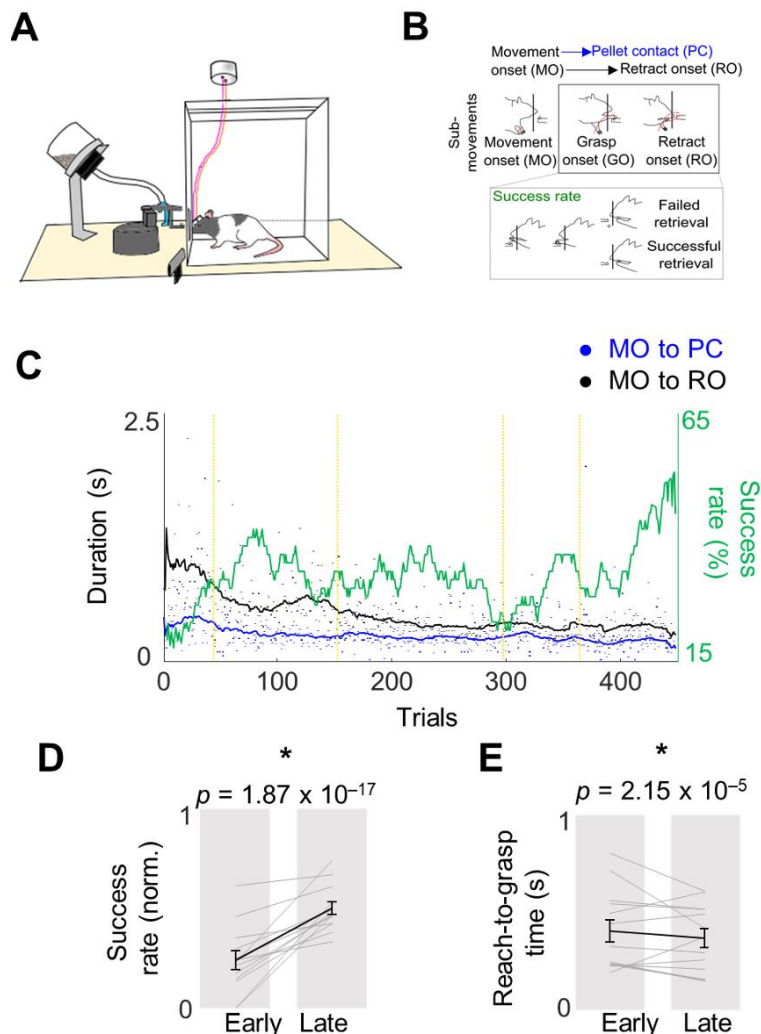
91

### 92 **Measurement of Skilled Motor Performance**

93 As in other studies that employ the Whishaw forelimb reach-to-grasp task, we assessed motor  
94 skill learning across two dimensions: speed and accuracy (**Fig. 1B-E**)<sup>3,50</sup>. Accuracy was measured  
95 as percent success in retrieving the pellet and speed was assessed using the time the animal  
96 took to perform the full reach-grasp-retract motor sequence. Training lasted for 5 days in  
97 automated behavioral boxes<sup>2,41</sup>, and animals performed 100–160 trials each day. Consistent with  
98 past results<sup>3,50</sup> over 5 days of learning, the success rate increased and movements became faster  
99 as measured through reach-grasp task completion duration or reach duration (see **Fig. 1**). On  
100 average, success rates increased from  $23.9 \pm 4.7\%$  to  $49.8 \pm 3.2\%$  from early to late days (mean

101  $\pm$  s.e.m., mixed-effects model:  $P = 1.87 \times 10^{-17}$ ) and reach duration came down from :  $406 \pm 57$   
102 ms on early days to  $367 \pm 48$  ms on late days (mean  $\pm$  s.e.m., mixed-effects model:  $P = 2.15 \times$   
103  $10^{-5}$ ).

104  
105 **Figure 1**



106  
107  
108 **Figure 1.** Behavioral evaluation of the skilled reach-to-grasp task. **A**, The behavioral setup for  
109 the skilled forelimb reaching task with simultaneous neurophysiological recording. **B**, Top:  
110 Illustration of the reach-to-grasp task showing the three major parts of the reach movement: reach  
111 onset, pellet contact, and retract onset. Bottom: Comparison of a failed trial and a successful trial.  
112 **C**, Success rate and reach event timing from a sample animal. **D,E**, Difference in success rate  
113 and reach duration from early training days to late training days ( $n = 13$  animals). Gray lines  
114 represent individual animals, and the black line is mean and s.e.m. across animals. P-values are  
115 from mixed-effects models.

116  
117

118 **Coordinated movement-related activity emerges across M1 and cerebellum during skill**  
119 **learning.**

120 We next evaluated the cerebellum in search of transient low-frequency oscillatory (LFO) dynamics  
121 similar to those that were recently shown to emerge in the M1<sup>2,3</sup> while learning this skill. We  
122 observed that coordinated LFO (1–4 Hz) activity appeared during movement across M1 and  
123 cerebellum as performance improved (**Fig. 2**). This low-frequency activity was clearly observed  
124 in movement-related LFP signals (**Fig 2B, C**). The movement-related LFP power in the LFO-band  
125 increased from early to late days in both M1 and cerebellum (**Fig. 2C**; M1 baseline-normalized  
126 power:  $0.51 \pm 0.15$  on early days to  $0.65 \pm 0.16$  on late days, mixed-effects model:  $t(406) = 4.3$ ,  
127  $P = 2.3 \times 10^{-5}$ ; cerebellum power:  $0.43 \pm 0.12$  to  $0.86 \pm 0.25$ , mixed-effects model:  $t(650) = 8.6$ ,  
128  $P = 8.4 \times 10^{-17}$ ).

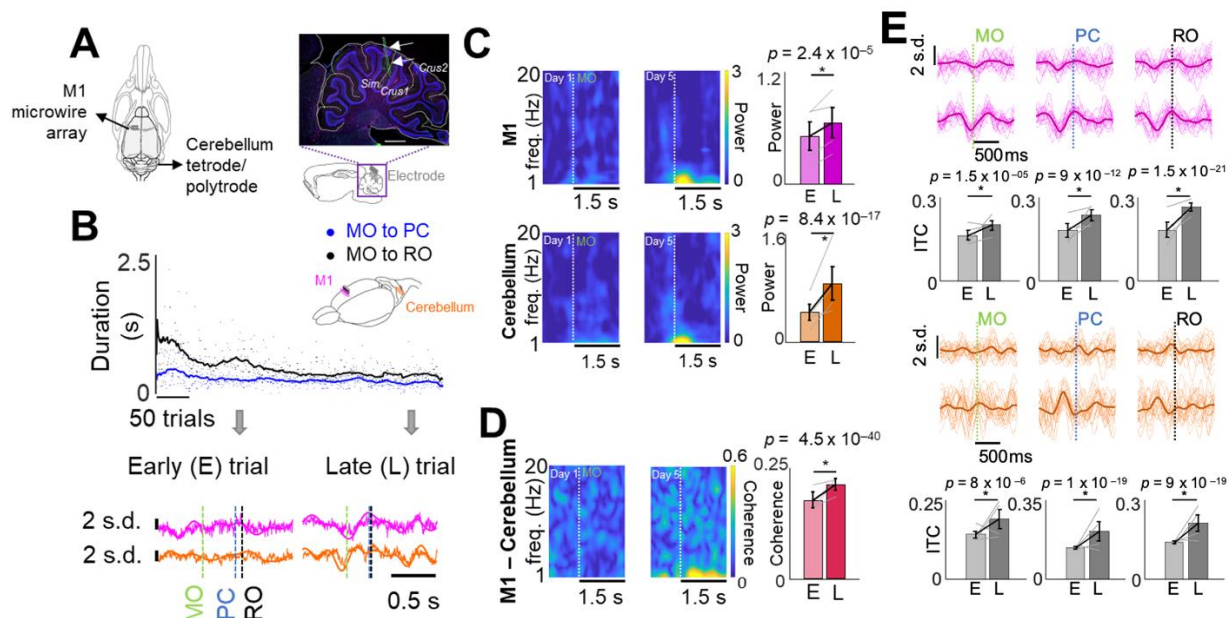
129  
130 We also analyzed movement-related low-frequency LFP coherence between M1 and cerebellum  
131 LFPs and we found that this also increased with increased task proficiency (**Fig. 2D**;  $0.18 \pm 0.02$   
132 coherence on early days to  $0.21 \pm 0.01$  on late days, mixed-effects model:  $t(5158) = 13.4$ ,  $P = 4.5$   
133  $\times 10^{-40}$ ). These increases in LFP power and coherence were not solely a by-product of faster and  
134 more consistent movements, since these high LFP power and coherence were not present for  
135 fast trials early in training, which we checked in a subset of animals.

136  
137 With training, reaching sub-movements also became precisely phase-locked to 1–4 Hz LFP  
138 signals in both M1 and cerebellum, consistent with what we would expect if this activity was  
139 involved in generating sub-movements within this task (**Fig. 2E**; significant increase in inter-trial  
140 coherence (ITC) of the M1 LFP locked to movement onset (*MO*): mixed-effects model:  $t(406) =$   
141  $4.4$ ,  $P = 1.5 \times 10^{-5}$ ; pellet contact (*PC*, right at the time of grasp initiation): mixed-effects model:  
142  $t(406) = 7.0$ ,  $P = 9.2 \times 10^{-12}$ ; and retract onset (*RO*): mixed-effects model:  $t(406) = 10.1$ ,  $P = 1.5$   
143  $\times 10^{-21}$ ; cerebellum LFP locked to movement onset: mixed-effects model:  $t(650) = 4.5$ ,  $P = 8 \times$

144  $10^{-6}$ , pellet touch: mixed-effects model:  $t(650) = 9.8$ ,  $P = 1 \times 10^{-19}$ , retract onset: mixed-effects  
 145 model:  $t(650) = 9.1$ ,  $P = 9.1 \times 10^{-19}$ .

146  
 147  
 148  
 149

## Figure 2



150  
 151  
 152 **Figure 2. Coordinated movement-related mesoscopic activity emerges across M1 and**  
 153 **cerebellum during skill learning. A, Left:** Schematic of recording electrode locations in M1 and  
 154 contralateral cerebellum depicted from top; **Right:** Histological verification of recording location in  
 155 cerebellum (three markers used: Iba1 (green, microglia), GFAP (pink, astrocytes), DAPI (blue,  
 156 nuclei). Sagittal section shows cerebellar lobules and cortical layers. Scale bar: 1 mm. Electrode  
 157 shank is marked by two arrows. **B, Top:** Example time course and illustration of recording scheme  
 158 in M1 and the cerebellum from a frontal-side view. **Bottom:** neural and forearm muscle activity for  
 159 representative successful trials from days 1 and 8. **C, Left:** Spectrograms of example M1 and  
 160 cerebellar channels. **Right:** Difference in 1–4 Hz cerebellum and M1 power from early training to  
 161 late training. The gray lines represent the mean power from individual animals ( $n = 4$  animals)  
 162 and the black lines represent the mean  $\pm$  s.e.m.  $P$ -values are from mixed-effects models. **D, Left:**  
 163 Coherograms from an example M1 and cerebellum LFP channel pair. **Right:** difference in 1–4 Hz  
 164 M1-cerebellum coherence from early to late training sessions. The gray lines represent the mean  
 165 coherence from individual animals ( $n = 3$  animals) and the black lines represent the mean and  
 166 s.e.m.  $P$ -values are from mixed-effects models. **E, 1–4 Hz filtered LFP** from example M1 and  
 167 cerebellum channels time-locked to reach events; individual trials with mean overlaid. Bar plots  
 168 depict changes in ITC from early trials to late trials (*upper row* for M1 and *lower row* for  
 169 cerebellum). The gray lines represent the mean ITC from individual animals ( $n = 4$  animals) and  
 170 the black lines represent the mean and s.e.m.  $P$ -values from mixed-effects models.

171  
 172  
 173



174

175 **Coordinated spiking activity emerges across M1 and cerebellum during skill learning.**

176 The emergence of coordinated low-frequency activity across M1 and cerebellum was also clearly  
177 observed in movement-related spiking activity across M1 and cerebellum. We quantified phase-  
178 locking of movement-related M1 and cerebellar spikes to 1–4 Hz LFP signals in each region by  
179 generating polar histograms of the LFP phase at which each spike occurred for a single unit and  
180 LFP channel (**Fig. 3A**). The non-uniformity of the distribution of phases (indicating phase-locking)  
181 was quantified using a Rayleigh test of circular non-uniformity. We compared all task-related M1  
182 and cerebellar units on day 1 and 5 to a representative LFP channel in M1 and cerebellum and  
183 observed an increase in the percentage of M1 and cerebellum units phase-locked to both M1 and  
184 cerebellum LFP signals with training (**Fig. 3B**; the black vertical dashed lines correspond to the  $P$   
185 = 0.05 significance threshold of the natural log of the Z statistic; M1 unit – M1 LFP pairs: 39.1%  
186 day 1 to 59.9% day 5,  $P = 8 \times 10^{-6}$ , Kolmogorov–Smirnov test; M1 unit – cerebellum LFP pairs:  
187 21.8–76.3%,  $P = 1.4 \times 10^{-30}$ , Kolmogorov–Smirnov test; cerebellum unit – M1 LFP pairs: 77.8–  
188 88.1%,  $P = 0.3$ , Kolmogorov–Smirnov test; cerebellum unit – cerebellum LFP pairs: 40.9–86.0%,  
189  $P = 2.3 \times 10^{-10}$ , Kolmogorov–Smirnov test). All the pairs showed a significantly increased phase-  
190 locking, except cerebellum unit–cerebellum LFP pairs, although they also trended in same  
191 direction over days. These results further suggest that coordinated low-frequency activity  
192 emerges across M1 and cerebellum during skill learning.

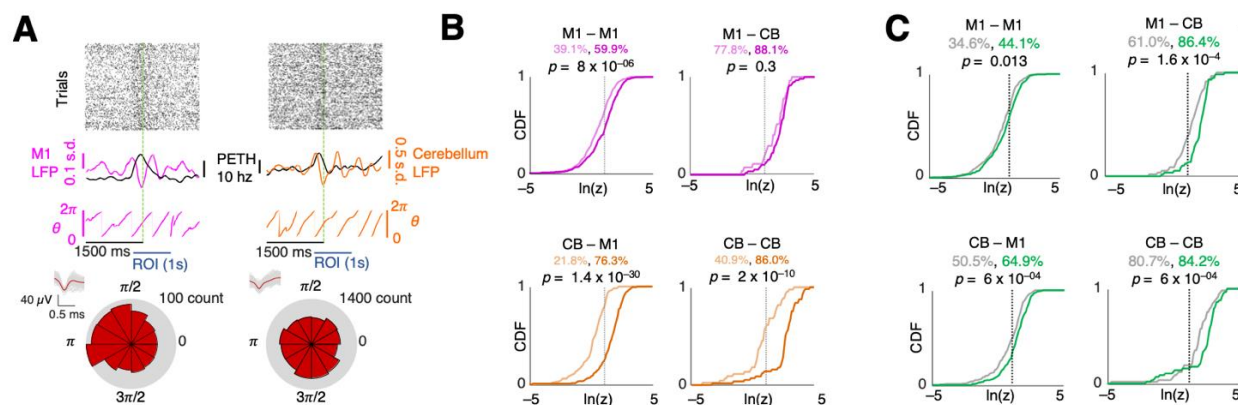
193

194 Next, we also explored these relations for successful and unsuccessful trials on day 5. We found  
195 that all four pairs showed significant M1 and cerebellar units' phase-locking to 1–4 Hz M1 and  
196 cerebellum LFPs for successful trials (**Fig. 3C**; the black vertical dashed lines correspond to the  
197  $P = 0.05$  significance threshold of the natural log of the Z statistic; M1 unit – M1 LFP pairs: 34.6%  
198 for unsuccessful trials versus 44.1% for successful trials,  $P = 0.013$ , Kolmogorov–Smirnov test;  
199 M1 unit – cerebellum LFP pairs: 50.5–64.9%,  $P = 6 \times 10^{-4}$ , Kolmogorov–Smirnov test; cerebellum

200 unit – M1 LFP pairs: 61.0–86.4%,  $P = 1.6 \times 10^{-4}$ , Kolmogorov–Smirnov test; cerebellum unit –  
 201 cerebellum LFP pairs: 80.7–84.2%,  $P = 2.3 \times 10^{-10}$ , Kolmogorov–Smirnov test).

202  
 203  
 204

### Figure 3



205  
 206

207 **Figure 3. Coordinated spiking activity emerges across M1 and cerebellum during skill**  
 208 **learning.** **A**, Illustration of spike locking to LFP phase for M1 unit-M1 LFP (left) and cerebellum  
 209 unit- cerebellum LFP (right) pair examples. *Top*: raster plots of reach-centered spiking activity  
 210 from example single units. *Middle*: 1–4 Hz filtered LFP overlaid with PETH from example unit.  
 211 Below is the extracted phase from the filtered LFP. *Bottom*. Polar histograms of the spikes that  
 212 occurred at various LFP phases. **B**, Cumulative density functions (CDFs) of the z-statistic for  
 213 every LFP-unit pair across and within each region. The vertical dotted lines indicate the  
 214 significance threshold ( $p = 0.05$ ). The percentage of the pairs with significant  $p$ -values is  
 215 displayed. Lighter colors indicate early trials and darker is later.  $n = 280$  M1 unit-LFP pairs on day  
 216 1,  $n = 298$  M1 unit-LFP pairs on day 5,  $n = 46$  cerebellum unit-LFP pairs on day 1,  $n = 73$   
 217 cerebellum unit-LFP pairs on day 5.  $P$ -values derived using a Kolmogorov-Smirnov test. **C**,  
 218 Success/failure CDFs of the z-statistic for every LFP-unit pair within and across each region. The  
 219 vertical dotted lines indicate the significance threshold ( $p = 0.05$ ). The percentage of the pairs  
 220 with significant  $p$ -values is displayed. Green indicate successful trials and gray is failures.  $P$ -  
 221 values derived using a Kolmogorov-Smirnov test.

222  
 223  
 224  
 225

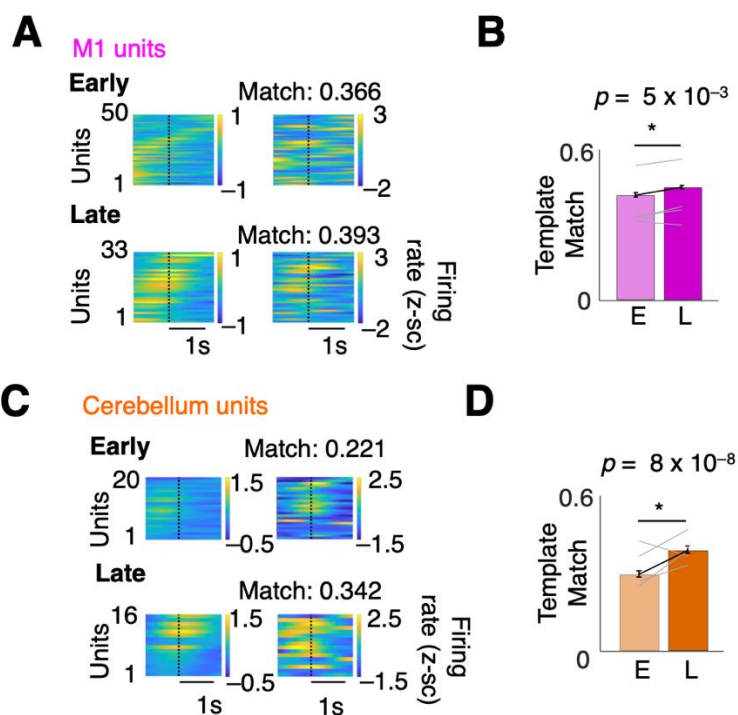
### Reorganization of neural dynamics in M1 and cerebellum with skill learning

226 We also investigated the consistency of single-trial population spiking activity by computing the  
 227 correlations between single-trial neural activity and the trial-averaged template across all units in  
 228 a session (**Fig. 4**). In early sessions, trial-to-trial neural firing was more inconsistent compared to  
 229 later sessions, while later sessions were consistently associated with a stereotyped sequence of  
 230 unit activations that also matched peri-event time histograms (PETH). This was observed in both

231 M1 (**Fig. 4A**) and cerebellar (**Fig. 4C**) activity. Across the sessions from all rats, we observed a  
232 significant increase in template correlation among trials (**Fig. 4B, D**; linear mixed-effects model.  
233 M1:  $t(770) = 8.2$ ,  $P = 5 \times 10^{-3}$ ), cerebellum:  $t(648) = 5.4$ ,  $P = 8 \times 10^{-8}$ ) indicating that trial-to-trial  
234 variability in M1 and cerebellum neural activity reduced with skill consolidation.

235  
236  
237

## Figure 4



238  
239  
240 **Figure 4. Changes in M1 and cerebellum neural dynamics with skill learning.** **A**, M1  
241 successful trial averaged PETH from an example rat (*left*) and single trial PETH example (*right*)  
242 for early (*top*) and late (*bottom*) training sessions. **B**, M1 PETH template match over training. Bars  
243 indicate mean  $\pm$  s.e.m. over trials. Gray lines indicate average per animal ( $n = 4$  animals).  $P$ -  
244 values are from mixed-effects models. **C**, Cerebellum successful trial-averaged PETH from an  
245 example rat (*left*) and single trial PETH example (*right*) for early (*top*) and late (*bottom*) training  
246 sessions. **D**, Cerebellum PETH template match over training. Bars indicate mean  $\pm$  s.e.m. over  
247 trials. Gray lines indicate average per animal ( $n = 4$  animals).

248  
249

## 250 Skilled movement representation in M1 and cerebellum

251 Lastly, we explored the representation of successful and failed reaches in M1 and cerebellum.

252 We used Gaussian-process factor analysis (GPFA) to find low-dimensional neural trajectory

253 representations of population spiking activity in M1 and cerebellum on individual trials<sup>3,51</sup> (**Fig. 5A**)  
254 and then compared trajectories for successful and unsuccessful trials in early and late learning.  
255 We observed a difference between trajectories for successful and unsuccessful trials in M1 and  
256 cerebellum. To compare successful and unsuccessful trials we computed the correlation between  
257 the mean neural trajectory for successful trials, that is, the ‘successful template’, and each  
258 individual trial’s neural trajectory (**Fig. 5B**) during the period from 250 ms before movement onset  
259 until 250ms after retract onset (**Fig. 5C**). This period encompassed the movement onset and pellet  
260 contact for grasping and retraction of the forelimb. Since trials differed in the duration of this  
261 period, we interpolated trajectories such that they were all the same length. Neural trajectories for  
262 unsuccessful trials had significantly lower correlation than successful trials (**Fig. 5C**, Early M1:  $P$   
263 =  $8.5 \times 10^{-12}$ , Early cerebellum:  $P = 0.02$ , Late M1:  $P = 1.1 \times 10^{-8}$ , Late cerebellum:  $6.6 \times 10^{-3}$   
264 mixed-effects model with Bonferroni correction for multiple comparisons). Together with Figure  
265 3c, this provided further evidence that accurate reach-to-grasp task execution has M1 and  
266 cerebellar reliance.

267

268

269

270

271

272

273

274

275

276

277

278

279

280

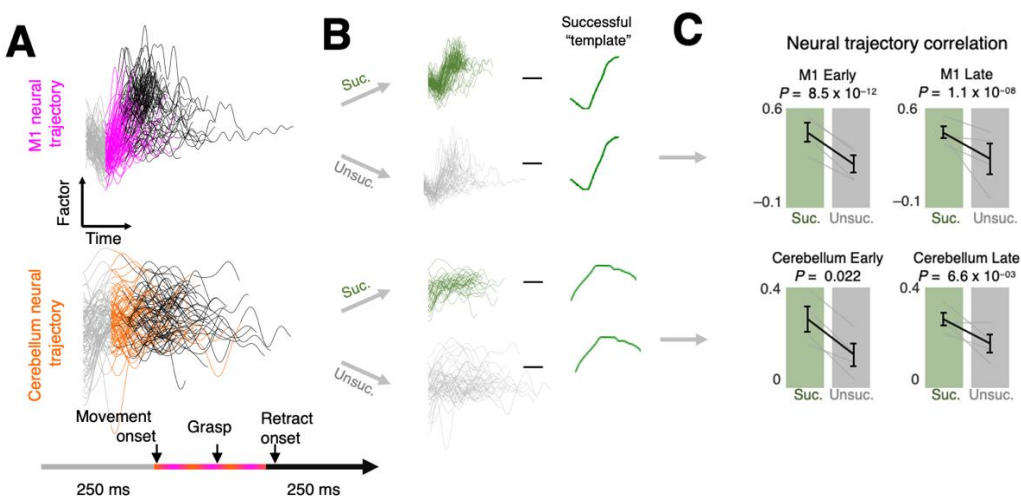
281

282

283

284 **Figure 5**

285



286

287

288 **Figure 5. Skilled movement representation in M1 and cerebellum.** **A**, Example GPFA neural  
289 trajectories from late training sessions for M1 (*top*) and cerebellum (*bottom*) in a single animal. **B**,  
290 Illustration of the process of comparing factor trajectories from successful and unsuccessful trials  
291 to the template (mean successful trajectory). **C**, Deviation from the template for M1 (*top*) and  
292 cerebellum (*bottom*) factors. Gray lines represent individual animals ( $n = 4$  animals), and the black  
293 line is mean  $\pm$  s.e.m. across animals.  $P$ -values are from mixed-effects models.

294

295

## 296 **Discussion**

297

298 In summary, we found that coordinated low-frequency activity emerged across M1 and  
299 cerebellum, which was linked to the emergence of faster reaching movements. We further found  
300 that coordinated spiking activity in both these regions was linked to accurate reach-to-grasp  
301 movements. Our work details the mesoscopic transmission in cortico-cerebellar networks and  
302 how it evolves with skill learning as well as how skilled reaching has a motor cortical and cerebellar  
303 cortical reliance.

304

### 305 ***Role of M1 and cerebellum in motor skill learning and execution***

306 M1 has a well-established role in motor learning as well as movement execution<sup>52</sup>. In particular,  
307 M1 is critical for generation of skilled dexterous movement<sup>13,20,43,52</sup>. Our work is consistent with this  
308 notion as we also see that M1 activity is different for successful reaches (**Fig. 3C, 4A and 5**). M1's  
309 projection to the cerebellum is thought to mediate fine-tuning of the movement. Cerebellar  
310 neurons in the cortex and in the deep nuclei are known to be modulated around several movement  
311 events. Perturbation of M1 input to cerebellum or direct manipulation of cerebellum itself is shown  
312 to delay movement initiation and to increase movement variability and duration<sup>13,34,37,53</sup>. Our work  
313 is also consistent with these observations as we found that precise, accurate movements had  
314 more consistent spiking activity in the cerebellum, and its coordination with LFOs in LFPs differed  
315 for successful and unsuccessful reaches (**Figs. 3C, 4B and 5**). Besides this role in increasing  
316 movement precision, cerebellar cortex is also theorized to contribute to task relevant  
317 dimensionality expansion that can aid in flexible computation and enhance learning<sup>54-56</sup>. This  
318 notion of dimensionality expansion was confirmed experimentally with the observations of high  
319 correlations among granule cells activity when mice expertly exerted pushing control over a  
320 manipulandum in a forelimb movement task<sup>11</sup>. This work also showed increase in emergent  
321 shared variance in M1 and cerebellar cells. Our increased M1-cerebellum LFP coherence with

322 skill learning is similar to this observation. Neural network models of cortico-cerebellar networks  
323 show that cerebellar feedback improves rate of learning and cerebellar network also carries task  
324 representation<sup>57</sup>. Our experimental data supports this notion as well. We observed that M1-  
325 cerebellum LFP coherence increased with learning, and we observed movement-modulated units  
326 in the cerebellum. One of our observations also showed that M1 LFP-cerebellar units showed  
327 strong coordination in low-frequency range early on in training (**Fig. 3B**). This might suggest that  
328 cerebellar activity was critical during reach-to-grasp skill acquisition and is consistent with the  
329 notions of M1 being input-driven, and is also consistent with the cerebellar contributions to  
330 acquisition of skilled volitional movements<sup>24,32</sup>.

331

### 332 ***Coordinated oscillatory dynamics across motor networks***

333 One of our key findings here is on low-frequency activity across M1 and cerebellum as an  
334 important marker of skilled motor control. We found evidence of such activity at the level of neural  
335 spiking and LFPs during the performance of dexterous task in rats. It is noteworthy that similar  
336 LFOs were recently shown to be disrupted in M1 post-stroke and tracked recovery<sup>2</sup>. This work  
337 also boosted M1 LFOs through electric stimulation to promote recovery. Recently, there has also  
338 been an interest in cerebellar stimulation for stroke recovery<sup>58-60</sup>, but a biomarker in cortico-  
339 cerebellar networks that can be target for closed-loop electric stimulation for stroke recovery is  
340 lacking. Future work can test if the LFOs we found in cortico-cerebellar networks of healthy  
341 animals with skill consolidation here can also serve as a biomarker for motor function during  
342 recovery from stroke. Mesoscopic biomarkers such as LFPs present a lower translational barrier  
343 in clinical populations.

344

345 Cortical LFOs can be used to decode reach-related activity and predict spiking phase across  
346 multiple behavioral states<sup>9,61</sup>. Such activity is also correlated with multiphasic muscle activations  
347 and timing of movements<sup>5,8,9,62</sup>. Recent work also suggest that oscillatory dynamics reflect an

348 underlying dynamical system<sup>5</sup>. This previous work argues that LFOs represent an intrinsic  
349 property of motor circuits associated with precise movement control. Our findings extend this body  
350 of work by showing LFO dynamics in both M1 and cerebellum (**Fig. 2**). The exact origin of LFOs  
351 and underlying generators remains unknown. While reach-related LFOs may have involved  
352 striatum<sup>3</sup> or thalamocortical activity<sup>63</sup> so far, our results here raise the possibility of cerebellar  
353 involvement. Further work can probe interactions between M1 and the broader motor network to  
354 pinpoint the drivers of the electrophysiologic changes seen during skill learning.



## 355 **Materials and Methods**

356

### 357 **Animal care and surgery**

358 All procedures were in accordance with protocols approved by the Institutional Animal Care and  
359 Use Committee at the Cedars-Sinai Medical Center. Adult male Long Evans rats (n = 13, 250–  
360 400 g; Charles River Laboratories) were housed in a 14-h/10-h light–dark cycle. All experiments  
361 were done during the light cycle. We used 8 rats for behavior only (**Fig. 1**) and 5 rats for behavior  
362 and physiology (**Figs. 2 to 5**; see **Supplementary Table 1** for details). No statistical methods  
363 were used to predetermine cohort size, but our sample sizes are similar to those reported in  
364 previous publications<sup>3,50,64–66</sup> (3–9 animals per group). Animals were pair-housed prior to  
365 electrode implantation or behavioral training and then single-housed after to prevent damage to  
366 implants, or to implement food restriction, respectively.

367

368 All surgical procedures were performed using sterile techniques under 1%–4% isoflurane.  
369 Surgery involved cleaning and exposure of the skull and preparation of the skull surface using  
370 cyanoacrylate and then implantation of the skull screws for referencing and overall head-stage  
371 stability. The analgesic regimen included the administration of 0.1 mg per kg body weight  
372 buprenorphine, and 5 mg per kg body weight carprofen. Neural implanted rats were also  
373 administered 2 mg per kg body weight dexamethasone and 33 mg per kg body weight sulfatrim  
374 for 5 days. All neural implanted animals were allowed to recover for 5 days prior to further  
375 behavioral training. Ground and reference screws were implanted posterior to lambda  
376 contralateral to the recorded cerebellum, contralateral to the neural recordings. For M1  
377 recordings, 32-channel arrays (33- $\mu$ m polyamide-coated tungsten microwire arrays) were lowered  
378 to a depth of ~1,200–1,500  $\mu$ m in either the left or right M1 depending on handedness. These  
379 were implanted centered at 0.5 mm anterior and 3 mm lateral to the bregma<sup>3,50</sup>. For cerebellar  
380 recordings we used 32-64 channel tetrodes (Neuronexus, MI) or shuttle-mounted polytrodes

381 (Cambridge Neurophysiology, UK). The probes were lowered into the cerebellar cortex through a  
382 craniotomy centered at 12.5 mm posterior and 2.5-3 mm lateral to bregma. Shuttle mounted  
383 probes were moved across days and recorded from depths of 1.5-4 mm. Our target regions were  
384 Simplex/ Crus I and Crus II areas of the cerebellum<sup>67-69</sup>. Activity in these areas has shown  
385 modulation during upper limb motor behaviors and in response to corticofugal fiber and forelimb  
386 stimulation. For the cerebellar recordings, we confirmed the location of electrode tips either  
387 through: (i) Staining with the orange/red fluorescence stain Dil (ThermoFisher Scientific) or (ii)  
388 three markers of Iba1 (microglia), GFAP (astrocytes), DAPI (nuclei) as shown in figure 2a (also  
389 see details below).

390  
391  
392

### Supplementary Table 1

Animal	Camera Frame rate (Hz)	M1 Probe	Electrode details	Cb Probe	Electrode details
1	30	Yes	32 channel array	Yes	8x4 Tetrode
2	75	Yes	32 channel array	Yes	4x16 Polytrode
3	75	Yes	32 channel array	Yes	4x16 Polytrode
4	75	Yes	32 channel array	No	N/A
5	87	No	N/A	Yes	2x32 Polytrode
6	30	No	N/A	No	N/A
7	30	No	N/A	No	N/A
8	30	No	N/A	No	N/A
9	30	No	N/A	No	N/A
10	30	No	N/A	No	N/A
11	30	No	N/A	No	N/A
12	87	No	N/A	No	N/A
13	87	No	N/A	No	N/A

393  
394  
395  
396  
397  
398  
399

**Supp. Table 1. Number of rats used for experiments.** Tabulated list of animals and behavioral monitoring camera frame rates and electrode used (see columns).

400 **Behavior**

401 ***Training***

402 Rats were acclimated to the behavioral box for at least 2 days and then exposed to a reach-to-  
403 grasp task for 5-10 trials to establish hand-preference before neural probe implantation. Probe  
404 implantation was performed in the contralateral M1 and ipsilateral cerebellum to the preferred  
405 hand. Rats were allowed to recover for at least 5 days before the start of experimental sessions.  
406 During behavioral assessments, we monitored the animals and ensured that their body weights  
407 did not drop below 90% of their initial weight. We used an automated reach-box, controlled by  
408 custom MATLAB scripts and an Arduino microcontroller. This setup requires minimal user  
409 intervention, as described previously<sup>41</sup>. Each trial consisted of a pellet dispensed on the pellet  
410 tray, followed by an alerting beep indicating that the trial was beginning. They then had 15 s to  
411 reach their arms through the slot, grasp and retrieve the pellet. A real-time 'pellet detector' using  
412 an infrared detector centered over the pellet was used to determine when the pellet was moved,  
413 which indicated that the trial was over, and the door was closed. All trials were captured by video  
414 through a camera placed on the side of the behavioral box. The camera was synced with the  
415 electrophysiology data either using Arduino digital output or directly through TTL pulses to the  
416 TDT RZ2 system. In electrode implanted animals the video frame rate ranged from 75-87 Hz  
417 aside from 1 animal for which the framerate was 30 Hz (see **Supp. Table 1**). For behavior-only  
418 animals the framerate was 30Hz aside from two animals for which the framerate was 87 Hz.

419

420 ***Behavioral Testing***

421 Rats began behavioral testing training 5 days after surgery by performing the same reach-to-  
422 grasp task. Electrophysiology recordings were taken throughout the full extent of the testing which  
423 consisted of one to two sessions of 60-100 trials per day for 5 days. Typically, each day would  
424 consist of a session of 100 trials followed by a session of 60 trials. Sessions within a day were  
425 spaced by a 2-hour resting block.

426

### 427 ***Behavioral analysis***

428 Behavioral analysis was done based on video recorded during experimental sessions. Reach  
429 videos were viewed and manually scored to obtain trial success, hand position and time points  
430 for reach onset, pellet contact and retract onset. To characterize motor performance, we  
431 quantified pellet retrieval success rate (percentage of pellets successfully retrieved into the box)  
432 and reach duration (time from reach onset to retract onset).

433

434

### 435 ***In vivo electrophysiology***

436 Units and LFP activity were recorded using a 128-channel TDT-RZ2 system (Tucker-Davis  
437 Technologies). Spike data were sampled at 24,414 Hz and LFP data at 1,017.3 Hz. ZIF (zero  
438 insertion force) clip-based digital head stages from TDT were used that interface the ZIF  
439 connector and the Intan RHD2000 chip that uses 192x gain. Behavior-related timestamps (that  
440 is, trial onset, trial completion) and video timestamps (that is, frame times) were sent to the RZ2  
441 analog input channel using an Arduino digital board and synchronized to the neural data.

442

443

### 444 ***Neural data analysis***

445 Analyses were conducted using custom-written scripts and functions in MATLAB 2018a  
446 (MathWorks, MA).

447

### 448 ***Local field potential (LFP) analyses***

449 Artifact rejection was first performed on LFP signals to remove broken channels and noisy trials.  
450 LFPs were then z-scored and median referenced separately for M1 and cerebellum. There was  
451 excessive noise detected in all cerebellum channels in 1 of the 4 animals with simultaneous M1

452 and cerebellum recordings. Hence, the cerebellar LFP activity from that animal was excluded  
453 from analysis. A fifth animal with only cerebellum implants was included in the cohort. LFP power  
454 was calculated on a trial-by-trial basis and then averaged across channels and animals, with  
455 wavelet decomposition using the EEGLAB<sup>70</sup> function 'newtimef'. To characterize coordination of  
456 activity across regions, we measured changes in movement-related spectral coherence between  
457 LFP channels in M1 and cerebellum. For learning comparisons, coherence was measured for the  
458 same channels on early and late days, and specifically for channels with an increase in power of  
459 0.5 baseline-normalized unit from early to late days. Strong coherence in a specific frequency  
460 band indicates a constant phase relationship in that frequency between two signals and is  
461 theorized to indicate increased communication between regions<sup>3,71,72</sup>. M1-cerebellum LFP  
462 coherence was calculated for each pair of channels using the EEGLAB function 'newcrossf' with  
463 0.1s windows moving by 0.01s.

464  
465 To determine whether the emergence of coordinated low-frequency activity during training was  
466 attributable solely to faster movements, we compared LFP power and coherence between 'fast'  
467 trials (trials with a movement duration less than 300 ms) on day 1 and 2 versus day 4 and 5.

468  
469 In several instances, we filtered the LFP signals to isolate and display the low-frequency (1–4 Hz)  
470 component of the signal (**Figs. 2 and 3**). Filtering was performed using the EEGLAB function  
471 'eegfilt'<sup>70</sup>. In addition to display purposes, we also used filtered LFP to characterize the phase-  
472 locking of spiking activity specifically to low-frequency LFP signals. For this we used the Hilbert  
473 transform linear operator (MATLAB) to extract the phase information from low- frequency filtered  
474 LFP signals (**Fig. 3**).

475  
476 To quantify phase-locking of LFP signals to specific sub-movements (movement onset, pellet  
477 contact and retract onset), we calculated the ITC of LFP signals across trials time-locked to these

478 sub-movements (**Fig. 2d**). ITC was measured and compared for the same channels on early and  
479 late days across all channels (except those removed due to noise). ITC was computed using the  
480 EEGLAB function 'newtimef'<sup>70</sup>.

481

### 482 ***Spiking analyses***

483 Spike data was sorted offline after local median subtraction. The threshold for spiking activity was  
484 set offline using the automated spike detection of Spyking Circus, and waveforms and timestamps  
485 were stored for any event that crossed that threshold. Sorting was performed using a principal  
486 component analysis (PCA)-based method followed by manual inspection and sorting. Clearly  
487 identified units were selected for this analysis. All units were analyzed and not sorted into cell  
488 type based on waveform shape. However, activity that was unambiguously multi-unit was  
489 removed. Behavior-related timestamps (trial onset and trial completion) were sent to the RZ2  
490 analog input channel using an Arduino digital board and synchronized to neural data.

491

### 492 ***Unit modulation and spike-LFP phase analysis***

493 Spikes were binned at 25 ms and time locked to behavioral markers. For visualization purposes,  
494 the peri-event time histogram (PETH) was estimated by the MATLAB 'fit' function using smoothing  
495 spines. To determine if a unit was significantly modulated during movement, a baseline firing rate  
496 mean and standard deviation was taken within the period -4s to -2s from reach onset. If the mean  
497 firing rate in the period from -350ms to -850ms relative to reach onset differed from the baseline  
498 mean by more than 1.25 baseline standard deviations the unit was categorized as a reach-  
499 modulated unit.

500

501 To characterize low-frequency spiking activity, we generated histograms of the LFP phases at  
502 which each spike occurred for a single unit to a single LFP channel filtered in the 1-4 Hz band in  
503 a 1-s window around movement (-250 ms before to 750 ms after movement onset) across all

504 trials of a session (**Fig. 3**). For learning comparisons, all units were compared to the same  
505 selected M1 and DLS LFP channel on day 1 and 5. These histograms were generated for each  
506 unit–LFP channel pair both within and across regions. For every pair, we then calculated the  
507 Rayleigh’s z-statistic for circular non-uniformity. These z-statistics were then used to calculate the  
508 percentage of significantly non-uniform distributions across unit–LFP pairs with a significance  
509 threshold of  $P = 0.05$  (**Fig. 3**). A significantly nonuniform distribution signifies phase preference  
510 for spikes of a unit to an LFP signal. This process was also performed to compare the successful  
511 and unsuccessful trials of day 5 (**Fig. 3C**).

512

### 513 ***Single trial to template correlation***

514 Spikes from  $-4$  s to  $4$  s around pellet touch were binned at 20 ms, smoothed with a Gaussian  
515 kernel with a standard deviation of 60 ms and then z-scored. Binned, smoothed and standardized  
516 spike counts within the period of  $-1$  s to  $1.25$  s for all units of a single trial were then concatenated  
517 into one long vector. The correlation (measured using Pearson’s  $r$ ) between each concatenated  
518 single trial neural activity and the mean template (mean of all successful trials) was computed  
519 and the mean correlation for each session was reported (**Fig. 4**).

520

### 521 ***GPFA neural trajectory analyses***

522 To characterize single-trial representations of population spiking activity we used GPFA<sup>3,51</sup> to find  
523 low-dimensional neural trajectories, which consisted of the first two factors, for each trial. GPFA  
524 analyses were carried out using the MATLAB based graphical user interface DataHigh (version  
525 1.2)<sup>73</sup>, 10 ms time bins and a dimensionality of 5. We determined the magnitude of deviation for  
526 each individual trial trajectory from the mean trajectory across all successful trials by taking the  
527 absolute value of the difference between the trajectory of each trial and the mean trajectory across  
528 all trials (**Fig. 5B, C**; computed in each dimension independently). This was performed specifically  
529 for the period between 250 ms before movement onset and until 250 ms after retract onset. Since

530 this duration varied across trials, we interpolated each trial such that every epoch (reach onset to  
531 touch and touch to retract onset) of each trial was the same length and then calculated the  
532 average deviation.

533

534

### 535 **Immunohistochemistry**

536 After all experiments, rats were anesthetized and transcardially perfused with 1% phosphate-  
537 buffered saline, followed by phosphate-buffered 4% formaldehyde (PFA). The harvested brains  
538 were post-fixed for 72 h in PFA and immersed in 30% sucrose. For immunofluorescence staining  
539 (**Fig. 2A**), sagittal cerebellar tissue cryostat sections (40  $\mu\text{m}$ ) were washed 3x in 1x Tris Buffered  
540 Saline (TBS), followed by antigen retrieval with 0.1N hydrochloric acid (HCl). After 3 more washes  
541 in 1xTBS, sections were blocked with 5% Normal Donkey Serum (NDS) in 0.1% TBS-T(Triton)  
542 for 1 hour. Sections were then incubated in primary antibodies for astrocytes and microglia  
543 overnight. The next day sections were washed 3 times in 1xTBS and then incubated with  
544 fluorescent secondary antibodies for 2 hours. Sections were then washed 3 times in 1xTBS and  
545 incubated with 300nM DAPI in 1xTBS for 7 min, before coverslipping with mounting media  
546 (ProLong<sup>TM</sup> Glass Antifade Mountant, ThermoFisher cat# P36980). Primary antibodies used are  
547 1:1000 Rat-anti-GFAP(ThermoFisher cat #13-0300) and 1:1000 Rabbit-anti-IBA1(Wako cat  
548 #019-19741). Secondary antibodies used are 1:250 Alexa Fluor<sup>TM</sup> 647 Donkey-anti Rat (Jackson  
549 cat# 712-605-153) and 1:1000 Alexa Fluor<sup>TM</sup> 488 Donkey-anti Rabbit 488(ThermoFisher cat #  
550 A-21206). Fluorescent sections were imaged with a BZ-X700 Keyence microscope.

551

552

### 553 **Statistical analysis**

554 The linear mixed-effects model (implemented using MATLAB 'fitlme') was used in this study.

555 Using these models accounts for the fact that units, channels or trials from the same animal are



556 more correlated than those from different animals; thus, it is more stringent than computing  
557 statistical significance over all units, channels or trials<sup>3,74</sup>. We fitted random intercepts for each rat  
558 and reported the p values for the regression coefficients associated with successful or  
559 unsuccessful outcome, early (that constituted days 1 and 2) or late (that constituted days 4 and  
560 5) learning, or training session. Linear mixed effects models was used for testing significance in  
561 **Figs 1D,E; 2C-E; 4B,D; and 5C**. Two-sample Kolmogorov–Smirnov tests were used to test  
562 whether spike-LFP phase-locking values on days 1 and 5 came from the same distribution (**Fig.**  
563 **3C**). All statistical analyses were implemented within MATLAB. We fitted random intercepts for  
564 each rat and reported the p values for the regression coefficients associated with successful or  
565 unsuccessful outcome, early or late learning, or training session.

566 **Acknowledgements**

567 We thank Celine Riera and Joshua Burda for resources and reagents for histology. We thank  
568 Keshav Suresh for assistance with immunohistochemistry. This research is supported by  
569 American Heart Association (postdoctoral fellowship 897265 to A.A. and career development  
570 award 847486 to T.G.), National Institutes of Health (R00NS097620 to T.G.), National Science  
571 Foundation (CAREER award 2048231 to T.G.) and Cedars-Sinai Medical Center. A.A. also  
572 received support from a Cedars-Sinai's Center for Neural Science and Medicine postdoctoral  
573 fellowship.

574

575

576

577 **Author Contributions**

578 P.J.F. and T.G. designed the study. P.J.F., A.A., A.W.F. and N.P.D. carried out the  
579 electrophysiology experiments. A.A., A.W.F., N.P.D. and T.G. performed the surgical procedures.  
580 P.J.F. carried out the analysis. A.A., A.W.F., N.P.D., R.S. and P.R.R. provided resources and  
581 assisted with analysis. A.W.F., N.P.D., R.S. and P.R.R. carried out histology. P.J.F. and T.G.  
582 wrote the manuscript. A.A. and A.W.F. edited the manuscript.

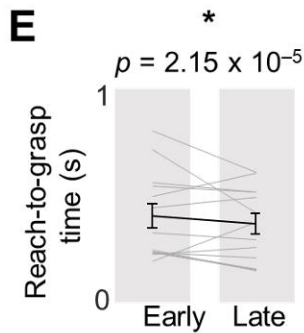
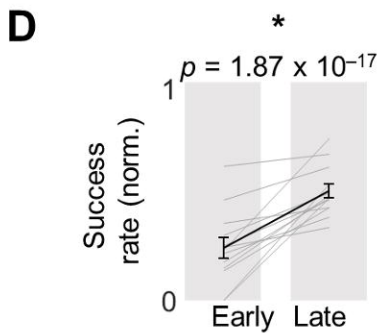
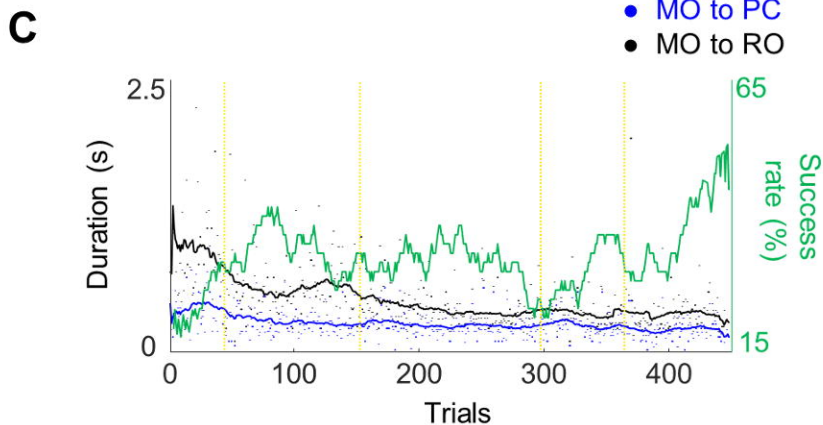
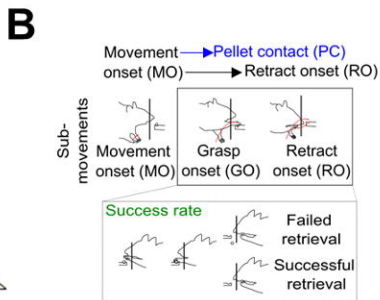
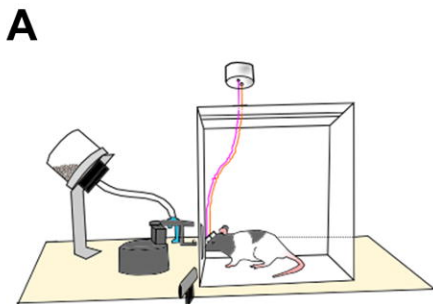
583 **References**

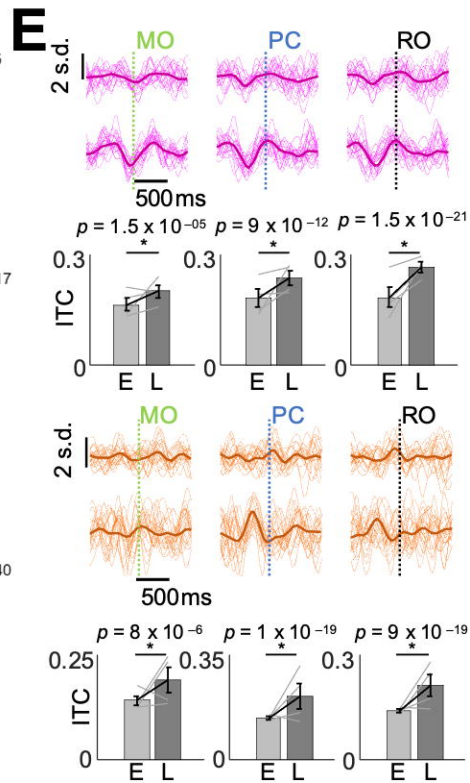
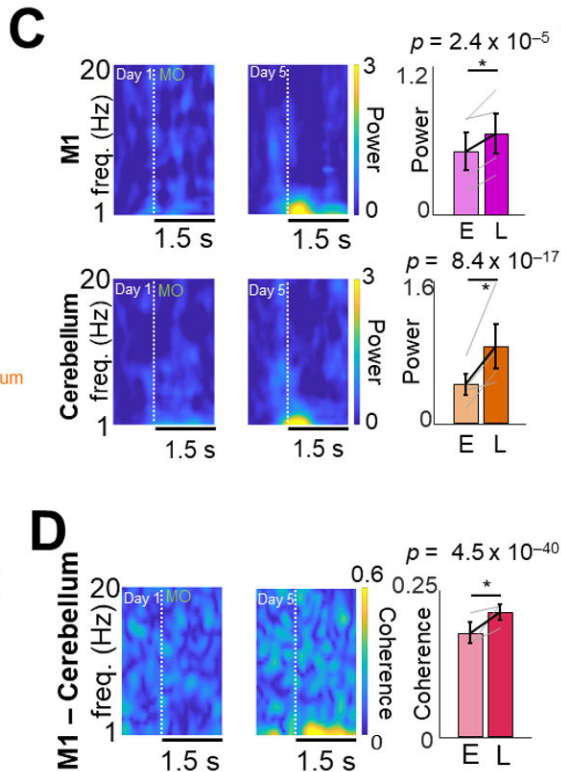
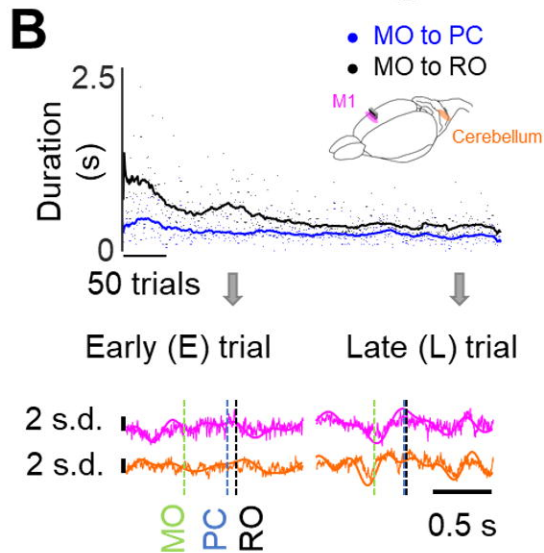
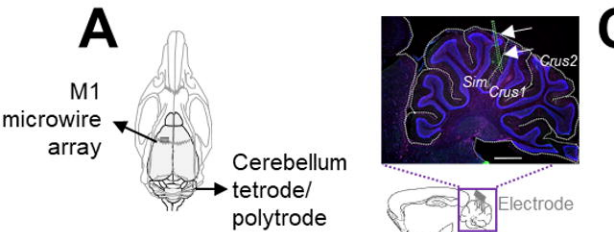
- 584 1. Hall, T. M., de Carvalho, F. & Jackson, A. A common structure underlies low-frequency  
585 cortical dynamics in movement, sleep, and sedation. *Neuron* vol. 83 1185–99 (2014).
- 586 2. Ramanathan, D. S. *et al.* Low-frequency cortical activity is a neuromodulatory target that  
587 tracks recovery after stroke. *Nat Med* **24**, 1257–1267 (2018).
- 588 3. Lemke, S. M., Ramanathan, D. S., Guo, L., Won, S. J. & Ganguly, K. Emergent modular  
589 neural control drives coordinated motor actions. *Nat Neurosci* vol. 22 1122–1131 (2019).
- 590 4. Churchland, M. M., Cunningham, J. P., Kaufman, M. T., Ryu, S. I. & Shenoy, K. V. Cortical  
591 preparatory activity: representation of movement or first cog in a dynamical machine? *Neuron*  
592 vol. 68 387–400 (2010).
- 593 5. Churchland, M. M. *et al.* Neural population dynamics during reaching. *Nature* vol. 487 51–6  
594 (2012).
- 595 6. Mollazadeh, M. *et al.* Spatiotemporal Variation of Multiple Neurophysiological Signals in the  
596 Primary Motor Cortex during Dexterous Reach-to-Grasp Movements. *J. Neurosci.* **31**, 15531–  
597 15543 (2011).
- 598 7. Donoghue, J. P., Sanes, J. N., Hatsopoulos, N. G. & Gaál, G. Neural Discharge and Local  
599 Field Potential Oscillations in Primate Motor Cortex During Voluntary Movements. *Journal of*  
600 *Neurophysiology* **79**, 159–173 (1998).
- 601 8. Stefanics, G. *et al.* Phase Entrainment of Human Delta Oscillations Can Mediate the Effects  
602 of Expectation on Reaction Speed. *J. Neurosci.* **30**, 13578–13585 (2010).
- 603 9. Hall, T. M., Nazarpour, K. & Jackson, A. Real-time estimation and biofeedback of single-  
604 neuron firing rates using local field potentials. *Nat Commun* **5**, 5462 (2014).
- 605 10. Kelly, R. M. & Strick, P. L. Cerebellar Loops with Motor Cortex and Prefrontal Cortex of a  
606 Nonhuman Primate. *J. Neurosci.* **23**, 8432–8444 (2003).
- 607 11. Wagner, M. J. *et al.* Shared Cortex-Cerebellum Dynamics in the Execution and Learning of a  
608 Motor Task. *Cell* vol. 177 669-682 e24 (2019).
- 609 12. Leergaard, T. B. *et al.* Three-dimensional topography of corticopontine projections from rat  
610 sensorimotor cortex: Comparisons with corticostriatal projections reveal diverse integrative  
611 organization. *Journal of Comparative Neurology* **478**, 306–322 (2004).
- 612 13. Guo, J.-Z. *et al.* Disrupting cortico-cerebellar communication impairs dexterity. *eLife* **10**,  
613 e65906 (2021).
- 614 14. Lawrence, D. G. & Kuypers, H. G. The functional organization of the motor system in the  
615 monkey. I. The effects of bilateral pyramidal lesions. *Brain* **91**, 1–14 (1968).
- 616 15. Whishaw, I. Q., Pellis, S. M., Gorny, B., Kolb, B. & Tetzlaff, W. Proximal and distal impairments  
617 in rat forelimb use in reaching follow unilateral pyramidal tract lesions. *Behav Brain Res* **56**,  
618 59–76 (1993).
- 619 16. Krakauer, J. W. & Carmichael, S. T. *Broken movement: the neurobiology of motor recovery*  
620 *after stroke*. (MIT Press, 2017).
- 621 17. Grünbaum, A. S. F. & Sherrington, C. S. Observations on the physiology of the cerebral cortex  
622 of some of the higher apes. (Preliminary communication.). *Proceedings of the Royal Society*  
623 *of London* **69**, 206–209 (1902).
- 624 18. Miri, A. *et al.* Behaviorally Selective Engagement of Short-Latency Effector Pathways by  
625 Motor Cortex. *Neuron* **95**, 683-696.e11 (2017).
- 626 19. Graziano, M. S. A., Taylor, C. S. R. & Moore, T. Complex movements evoked by  
627 microstimulation of precentral cortex. *Neuron* **34**, 841–851 (2002).
- 628 20. Guo, J.-Z. *et al.* Cortex commands the performance of skilled movement. *eLife* **4**, e10774.
- 629 21. Scott, S. H. The role of primary motor cortex in goal-directed movements: insights from  
630 neurophysiological studies on non-human primates. *Curr Opin Neurobiol* **13**, 671–677 (2003).
- 631 22. Georgopoulos, A. P., Kalaska, J. F., Caminiti, R. & Massey, J. T. On the relations between  
632 the direction of two-dimensional arm movements and cell discharge in primate motor cortex.  
633 *J Neurosci* **2**, 1527–1537 (1982).

- 634 23. Evarts, E. V. Pyramidal tract activity associated with a conditioned hand movement in the  
635 monkey. *Journal of Neurophysiology* **29**, 1011–1027 (1966).
- 636 24. Sauerbrei, B. A. *et al.* Cortical pattern generation during dexterous movement is input-driven.  
637 *Nature* **577**, 386–391 (2020).
- 638 25. Bollu, T. *et al.* Motor cortical inactivation reduces the gain of kinematic primitives in mice  
639 performing a hold-still center-out reach task. 304907 (2018) doi:10.1101/304907.
- 640 26. Fortier, P. A., Kalaska, J. F. & Smith, A. M. Cerebellar neuronal activity related to whole-arm  
641 reaching movements in the monkey. *J Neurophysiol* vol. 62 198–211 (1989).
- 642 27. Thach, W. T. Discharge of cerebellar neurons related to two maintained postures and two  
643 prompt movements. I. Nuclear cell output. *J Neurophysiol* vol. 33 527–36 (1970).
- 644 28. Wetts, R., Kalaska, J. F. & Smith, A. M. Cerebellar nuclear cell activity during antagonist  
645 cocontraction and reciprocal inhibition of forearm muscles. *J Neurophysiol* vol. 54 231–44  
646 (1985).
- 647 29. HECK, D., KUMMELL, F., THACH, W. T. & AERTSENA, A. Dynamic Correlation of Neuronal  
648 Activity in Rat Cerebellar Cortex Modulated by Behavior. *Annals of the New York Academy  
649 of Sciences* vol. 978 156–163 (2002).
- 650 30. van Kan, P. L., Gibson, A. R. & Houk, J. C. Movement-related inputs to intermediate  
651 cerebellum of the monkey. *J Neurophysiol* vol. 69 74–94 (1993).
- 652 31. Marple-Horvat, D. E. & Stein, J. F. Cerebellar neuronal activity related to arm movements in  
653 trained rhesus monkeys. *J Physiol* vol. 394 351–66 (1987).
- 654 32. Bloedel, J. R., Bracha, V., Milak, M. & Shimansky, Y. Cerebellar contributions to the  
655 acquisition and execution of learned reflex and volitional movements. *Prog Brain Res* vol. 114  
656 499–509 (1997).
- 657 33. Thach, W. T. What is the role of the cerebellum in motor learning and cognition? *Trends in  
658 Cognitive Sciences* vol. 2 331–337 (1998).
- 659 34. Nashef, A., Cohen, O., Harel, R., Israel, Z. & Prut, Y. Reversible Block of Cerebellar Outflow  
660 Reveals Cortical Circuitry for Motor Coordination. *Cell Reports* **27**, 2608-2619.e4 (2019).
- 661 35. Tseng, Y., Diedrichsen, J., Krakauer, J. W., Shadmehr, R. & Bastian, A. J. Sensory Prediction  
662 Errors Drive Cerebellum-Dependent Adaptation of Reaching. *Journal of Neurophysiology* **98**,  
663 54–62 (2007).
- 664 36. Zackowski, K. M., Thach, W. T. & Bastian, A. J. Cerebellar subjects show impaired coupling  
665 of reach and grasp movements. *Exp Brain Res* **146**, 511–522 (2002).
- 666 37. Becker, M. I. & Person, A. L. Cerebellar Control of Reach Kinematics for Endpoint Precision.  
667 *Neuron* vol. 103 335-348 e5 (2019).
- 668 38. Galea, J. M., Vazquez, A., Pasricha, N., de Xivry, J. J. & Celnik, P. Dissociating the roles of  
669 the cerebellum and motor cortex during adaptive learning: the motor cortex retains what the  
670 cerebellum learns. *Cereb Cortex* vol. 21 1761–70 (2011).
- 671 39. Herzfeld, D. J. *et al.* Contributions of the cerebellum and the motor cortex to acquisition and  
672 retention of motor memories. *Neuroimage* vol. 98 147–58 (2014).
- 673 40. Whishaw, I. Q. & Pellis, S. M. The structure of skilled forelimb reaching in the rat: a proximally  
674 driven movement with a single distal rotatory component. *Behav Brain Res* **41**, 49–59 (1990).
- 675 41. Wong, C. C., Ramanathan, D. S., Gulati, T., Won, S. J. & Ganguly, K. An automated  
676 behavioral box to assess forelimb function in rats. *Journal of neuroscience methods* vol. 246  
677 30–7 (2015).
- 678 42. Gulati, T. *et al.* Robust neuroprosthetic control from the stroke perilesional cortex. *The Journal  
679 of Neuroscience* vol. 35 8653–61 (2015).
- 680 43. Iwaniuk, A. N. & Whishaw, I. Q. On the origin of skilled forelimb movements. *Trends Neurosci*  
681 **23**, 372–376 (2000).
- 682 44. Klein, A., Sacrey, L. A., Whishaw, I. Q. & Dunnett, S. B. The use of rodent skilled reaching as  
683 a translational model for investigating brain damage and disease. *Neurosci Biobehav Rev* vol.  
684 36 1030–42 (2012).

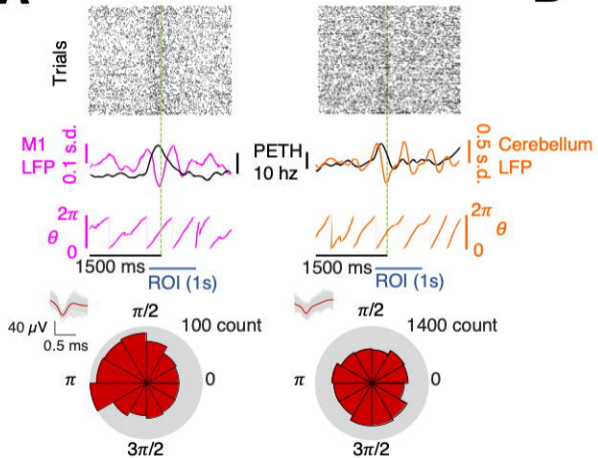
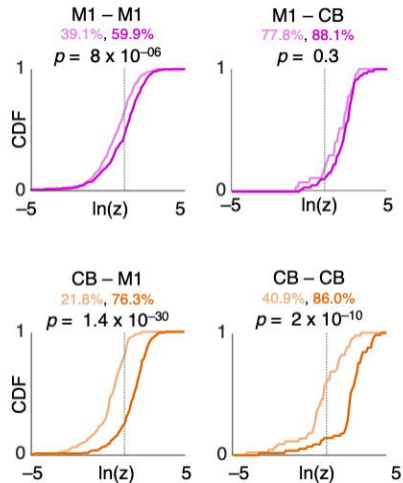
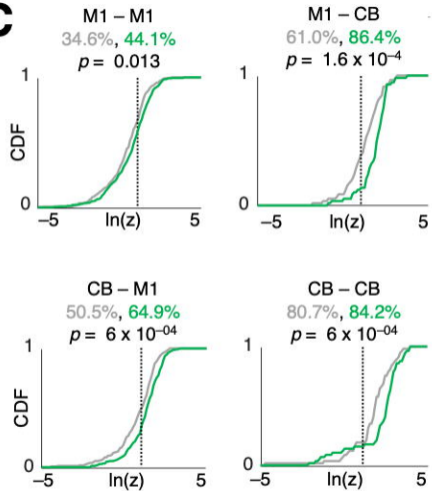
- 685 45. Rioult-Pedotti, M. S., Friedman, D. & Donoghue, J. P. Learning-induced LTP in neocortex.  
686 *Science* **290**, 533–536 (2000).
- 687 46. Fu, M., Yu, X., Lu, J. & Zuo, Y. Repetitive motor learning induces coordinated formation of  
688 clustered dendritic spines in vivo. *Nature* **483**, 92–95 (2012).
- 689 47. Kleim, J. A., Barbay, S. & Nudo, R. J. Functional reorganization of the rat motor cortex  
690 following motor skill learning. *J Neurophysiol* vol. 80 3321–3325 (1998).
- 691 48. Calame, D. J., Becker, M. I. & Person, A. L. Cerebellar associative learning underlies skilled  
692 reach adaptation. 2021.12.17.473247 (2021) doi:10.1101/2021.12.17.473247.
- 693 49. Sathian, K. *et al.* Neurological principles and rehabilitation of action disorders: common  
694 clinical deficits. *Neurorehabil Neural Repair* **25**, 21S–32S (2011).
- 695 50. Ramanathan, D. S., Gulati, T. & Ganguly, K. Sleep-Dependent Reactivation of Ensembles in  
696 Motor Cortex Promotes Skill Consolidation. *PLoS Biol* vol. 13 e1002263 (2015).
- 697 51. Yu, B. M. *et al.* Gaussian-Process Factor Analysis for Low-Dimensional Single-Trial Analysis  
698 of Neural Population Activity. *Journal of Neurophysiology* **102**, 614–635 (2009).
- 699 52. Peters, A. J., Liu, H. & Komiyama, T. Learning in the Rodent Motor Cortex. *Annual Review of*  
700 *Neuroscience* **40**, 77–97 (2017).
- 701 53. Conrad, B. & Brooks, V. B. Effects of dentate cooling on rapid alternating arm movements.  
702 *Journal of Neurophysiology* **37**, 792–804 (1974).
- 703 54. Albus, J. S. A theory of cerebellar function. *Mathematical Biosciences* **10**, 25–61 (1971).
- 704 55. Marr, D. A theory of cerebellar cortex. *The Journal of Physiology* **202**, 437–470 (1969).
- 705 56. Litwin-Kumar, A., Harris, K. D., Axel, R., Sompolinsky, H. & Abbott, L. F. Optimal Degrees of  
706 Synaptic Connectivity. *Neuron* **93**, 1153–1164.e7 (2017).
- 707 57. Boven, E., Pemberton, J., Chadderton, P., Apps, R. & Costa, R. P. Cerebro-cerebellar  
708 networks facilitate learning through feedback decoupling. 2022.01.28.477827 (2022)  
709 doi:10.1101/2022.01.28.477827.
- 710 58. Abbasi, A. *et al.* Epidural cerebellar stimulation drives widespread neural synchrony in the  
711 intact and stroke perilesional cortex. *Journal of NeuroEngineering and Rehabilitation* **18**, 89  
712 (2021).
- 713 59. Machado, A. G., Baker, K. B., Schuster, D., Butler, R. S. & Rezai, A. Chronic electrical  
714 stimulation of the contralesional lateral cerebellar nucleus enhances recovery of motor  
715 function after cerebral ischemia in rats. *Brain Res* vol. 1280 107–116 (2009).
- 716 60. Shah, A. M. *et al.* Optogenetic neuronal stimulation of the lateral cerebellar nucleus promotes  
717 persistent functional recovery after stroke. *Sci Rep* vol. 7 46612 (2017).
- 718 61. Mollazadeh, M. *et al.* Coherency between spike and LFP activity in M1 during hand  
719 movements. in *2009 4th International IEEE/EMBS Conference on Neural Engineering* 506–  
720 509 (2009). doi:10.1109/NER.2009.5109344.
- 721 62. Flint, R. D., Ethier, C., Oby, E. R., Miller, L. E. & Slutzky, M. W. Local field potentials allow  
722 accurate decoding of muscle activity. *J Neurophysiol* vol. 108 18–24 (2012).
- 723 63. Dossi, R. C., Nuñez, A. & Steriade, M. Electrophysiology of a slow (0.5–4 Hz) intrinsic  
724 oscillation of cat thalamocortical neurones in vivo. *J Physiol* **447**, 215–234 (1992).
- 725 64. Gulati, T., Guo, L., Ramanathan, D. S., Bodepudi, A. & Ganguly, K. Neural reactivations  
726 during sleep determine network credit assignment. *Nature Neuroscience* vol. 20 1277–1284  
727 (2017).
- 728 65. Kargo, W. J. & Nitz, D. A. Improvements in the signal-to-noise ratio of motor cortex cells  
729 distinguish early versus late phases of motor skill learning. *J Neurosci* vol. 24 5560–5569  
730 (2004).
- 731 66. Sauerbrei, B. A., Lubenov, E. V. & Siapas, A. G. Structured variability in Purkinje cell activity  
732 during locomotion. *Neuron* **87**, 840–852 (2015).
- 733 67. Heck, D. H., Thach, W. T. & Keating, J. G. On-beam synchrony in the cerebellum as the  
734 mechanism for the timing and coordination of movement. *Proc Natl Acad Sci U S A* vol. 104  
735 7658–63 (2007).

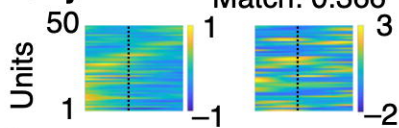
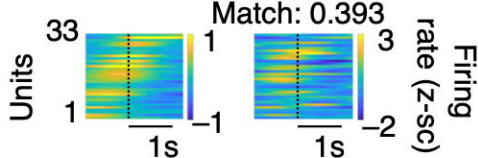
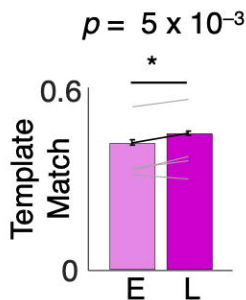
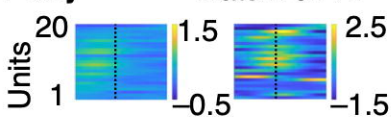
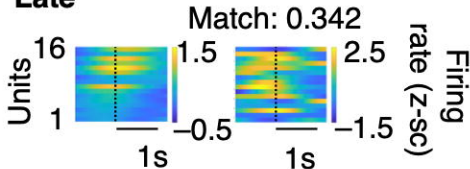
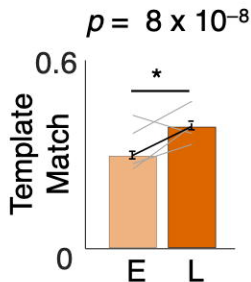
- 736 68. Atkins, M. J. & Apps, R. Somatotopical organisation within the climbing fibre projection to the  
737 paramedian lobule and copula pyramidis of the rat cerebellum. *J Comp Neurol* vol. 389 249–  
738 63 (1997).
- 739 69. Baker, M. R., Javid, M. & Edgley, S. A. Activation of cerebellar climbing fibres to rat cerebellar  
740 posterior lobe from motor cortical output pathways. *J Physiol* vol. 536 825–39 (2001).
- 741 70. Delorme, A. & Makeig, S. EEGLAB: an open source toolbox for analysis of single-trial EEG  
742 dynamics including independent component analysis. *Journal of Neuroscience Methods* **134**,  
743 9–21 (2004).
- 744 71. Fries, P. A mechanism for cognitive dynamics: neuronal communication through neuronal  
745 coherence. *Trends in Cognitive Sciences* **9**, 474–480 (2005).
- 746 72. Fries, P. Rhythms for Cognition: Communication through Coherence. *Neuron* **88**, 220–235  
747 (2015).
- 748 73. Cowley, B. R. *et al.* DataHigh: graphical user interface for visualizing and interacting with high-  
749 dimensional neural activity. *J. Neural Eng.* **10**, 066012 (2013).
- 750 74. Aarts, E., Verhage, M., Veenvliet, J. V., Dolan, C. V. & van der Sluis, S. A solution to  
751 dependency: using multilevel analysis to accommodate nested data. *Nat Neurosci* vol. 17  
752 491–6 (2014).
- 753

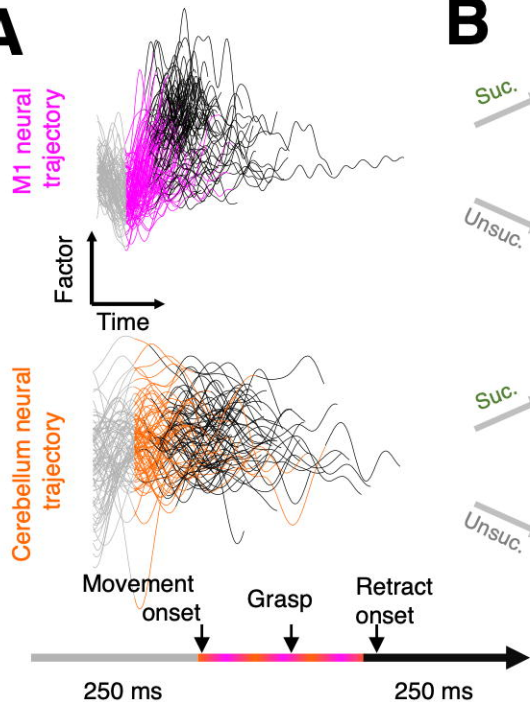
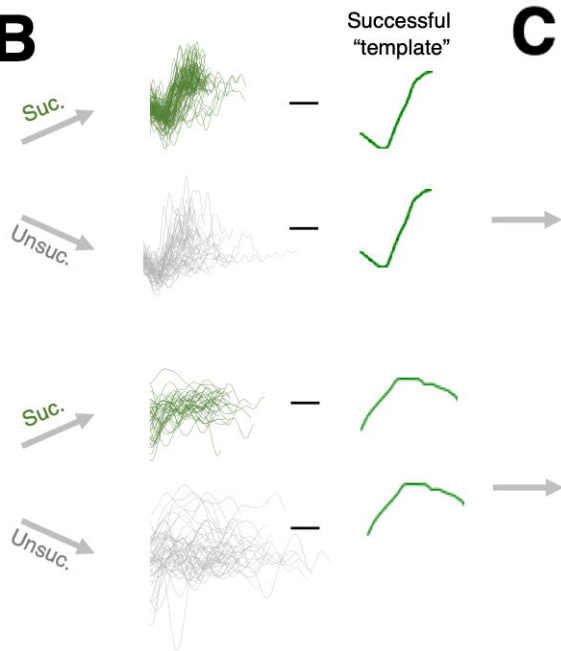






**A****B****C**

**A****M1 units****Early****Late****B****C****Cerebellum units****Early****Late****D**

**A****B****C**